

# Local Mean and Pattern Standard Deviation Map for Disease Staging in Glaucoma

Dennis C. Mock<sup>a</sup>

<sup>a</sup>David Geffen UCLA School of Medicine, University of California, Los Angeles, 10833 Le Conte Ave, Los Angeles, CA 90095

1 Correspondence: [dmock@ucla.edu](mailto:dmock@ucla.edu)

2

3 **Abstract.** For monitoring disease progression in glaucoma, perimetric measurements as global indices such as the mean deviation and standard pattern deviation for the visual field perimetry do not maintain a consistent diagnostic sensitivity over the entire data range. Here an analytical approach that assumes an underlying Gaussian mixture model describing the normal visual field offers an alternative solution to this situation.

11

12 Glaucoma is a multi-factorial eye disease that involves the degeneration of the optic nerve which leads to blindness. For this disorder, the visual function deteriorates mainly due to the death of the retinal ganglion cells and of the axons surrounding the optic nerve. It is known that particular measurements such as the mean deviation (MD) and standard pattern deviation (PSD) for the visual field (VF) perimetry do not maintain a consistent monotonic diagnostic sensitivity over the entire VF range (e.g. -33 to 0 [dB]) when monitoring the disease progression in glaucoma (1)(2)(3). Specifically, the MD is less sensitive for detecting disease related changes in the VF observed at the earlier stages (e.g. pre-perimetric, -2 to 0 [dB]), with the PSD similarly becoming less sensitive as an indicator for VF changes seen in the later stages of the disease progression (e.g. MD less than -15 dB).

28 There are many technical and statistical issues why this happens, leading to the standard paradigms for how the MD and PSD are used as statistical classifiers for glaucoma (4). Data analyses to reformulate the VF location sensitivity values as readout parameters like the pattern deviation (PD) and general height (GH) into separate VF spatial components may directly address some of these issues (5). For these reasons, the MD and PSD are considered as VF summary indices not intended generally for diagnosis but simply for disease staging (6).

41 As displayed in Figure 1, the scatterplot from the University of Washington VF supplemental dataset on GITHUB shows this common relationship for the PSD vs MD (MTD) from a large dataset (7, 8). Here, as the visual

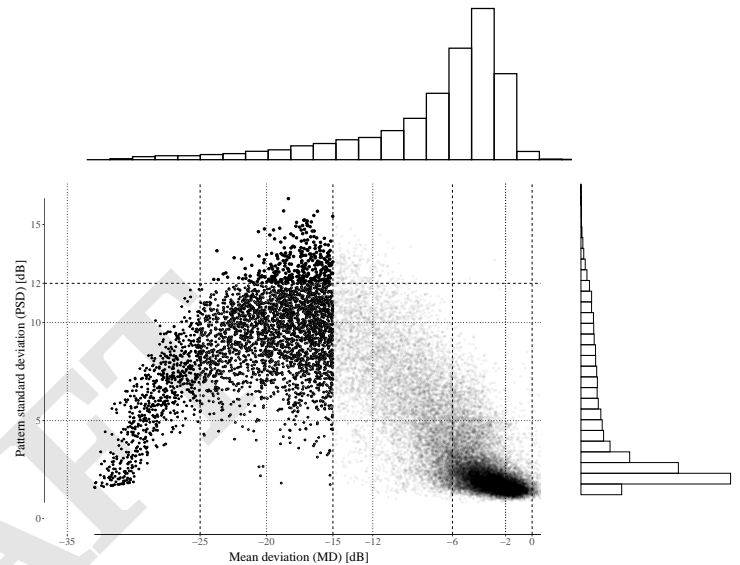


**Fig. 1.** The plot displaying the pattern standard (PSD) vs mean (MD) deviation (n=28,943) from the U.W. glaucoma perimetry dataset. The VF subsets are indicated by the symbols:

•  $-25 < MD \leq -15, 12 \leq PSD [dB]$  ○  $-25 < MD \leq -15, 12 > PSD [dB]$  •  $MD \leq -25 [dB]$  ○  $MD > -15 [dB]$

field damage progresses, as indicated with the MD decreasing, a reduction in diagnostic sensitivity is observed with the PSD value eventually declining after initially increasing with disease progression (3).

Given the evidence that the functional information derived from VF perimetry corresponds to the structural abnormalities between matching spatial regions, recomposing the global indices MD, PSD as local, spatial indices may provide more relevant readouts for staging the disease for glaucoma (9, 10).

For instance, suppose one defines the spatial regions of an individual VF with the Garway-Heath (GH) sectors (11, 12). Then by calculating the mean ( $MD_{sec}$ ) and pattern standard deviation ( $PSD_{sec}$ ) for each of the GH sectors, the VF summary statistics ( $MD_{loc}$ ,  $PSD_{loc}$ ) for

The author has no competing interests.

61 each VF is composed of separate components with its  
 62 corresponding individual  $MD_{sec}$  and  $PSD_{sec}$  for each  
 63 VF. Subsequently the components may be combined,  
 64 for example, or summed as a total summary statistic,  
 65  $MD_{loc}$  and  $PSD_{loc}$ , respectively.

66  
 67 For example, new summary indices are, for the *local*  
 68 mean deviation:

$$69 \quad MD_{loc} = MD_{i_{10}} + MD_{i_{15}} + MD_{i_{20}} + MD_{i_{25}} + MD_{i_{30}} + MD_{i_{35}}$$

70  
 71 and for the *local* pattern standard deviation:

$$72 \quad PSD_{loc} = \sqrt{PSD_{i_{10}}^2 + PSD_{i_{15}}^2 + PSD_{i_{20}}^2 + PSD_{i_{25}}^2 + PSD_{i_{30}}^2 + PSD_{i_{35}}^2}$$

73  
 74  
 75 Given the original statistical formula for the MD for a  
 76 single VF is defined as (13):

$$77 \quad \underbrace{\left[ \frac{1}{n} \sum_{i=1}^n \frac{(X_i - N_i)}{s_{1i}^2} \right]}_{MD_{sec} [dB] \text{ for specific } n \text{ by sector}} \bigg/ \left[ \frac{1}{n} \sum_{i=1}^n \frac{1}{s_{1i}^2} \right]$$

78 the statistical formula for calculating the new  $MD_{loc}$  is  
 79 now

$$80 \quad MD_{loc} = MD$$

81 since the calculation is mathematically linear with the  
 82 "mean of the sums" being equivalent to the "sum of the  
 83 means" for each individual VF.

84  
 85 However, the statistical derivation of the  $PSD_{loc}$   
 86 shows the mathematical equation is non-linear and  
 87 depends on the values of the local  $MD_{sec}$  (13). There-  
 88 fore the sum of the TD components relative to a new  
 89 calculation of the  $MD_{sec}$  would yield a different final  
 90 summation value for  $PSD_{loc}$ .

$$91 \quad PSD_{loc} = \sqrt{\overbrace{\left[ \frac{1}{n} \sum_{i=1}^n s_{1i}^2 \right]}_{PSD_{sec} [dB] \text{ for specific } n \text{ by sector}} \left[ \frac{1}{n-1} \sum_{i=1}^n \frac{(X_i - N_i - MD_{sec})^2}{s_{1i}^2} \right]}$$

92 Therefore

$$93 \quad PSD_{loc} \neq PSD$$

94 and plotting the  $PSD_{loc}$  value vs the MD (or  $MD_{loc}$ )  
 95 does not diminish as the MD becomes increasingly more  
 96 negative (see Figure 2). Statistically, this may be under-  
 97 stood by examining the distributions of the location sensi-  
 98 tivities from a normal perimetry database on the individ-  
 99 ual GH sectors (see Figure 3). The overlapping Gaussian  
 100 normal sub-distribution for each GH sector have varying

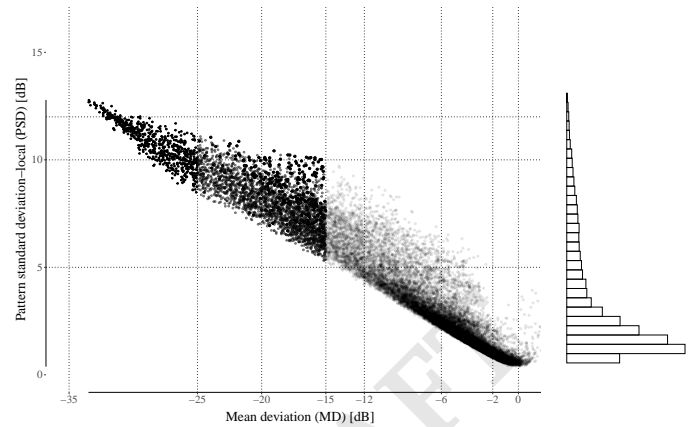


Fig. 2. The plot displaying the pattern standard ( $PSD_{loc}$ ) deviation ( $n=28,943$ ) from the U.W. glaucoma perimetry dataset. The VF subsets are indicated by the symbols:

- $-25 < MD \leq -15, 12 \leq PSD [dB]$
- $-25 < MD \leq -15, 12 > PSD [dB]$
- $MD \leq -25 [dB]$
- $MD > -15 [dB]$

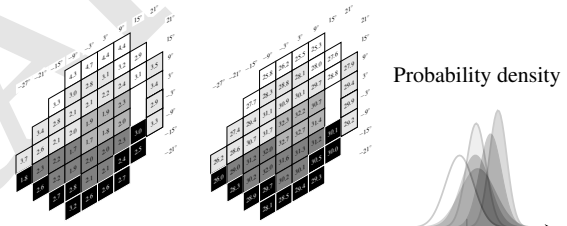


Fig. 3. The standard deviation and normal mean thresholds, resp. with values from the literature (17) (left, middle). A graph of a Gaussian mixture model based on the normal means and standard deviations by GH sector. (right)

101 statistical parameters,  $N(\mu, \sigma^2)$ . Therefore a VF statisti-  
 102 cal model may be represented here as a Gaussian mixture  
 103 model with the varying  $MD_{sec}$  for each GH sector (14-  
 104 16). This would computationally account for an increase  
 105 in detecting local changes for the individual  $PSD_{sec}$  as  
 106 one would expect from calculating the VF location sensi-  
 107 tivities from the local sector rather than global VF  
 108 means.

109 The revised statistical formulas for the  $MD_{sec}$  and  
 110  $PSD_{sec}$  for each Garway-Heath sector are shown pictori-  
 111 ally in Table 1 with the individual standard deviations  
 112 for the VF locations obtained from the literature (17).

It is made available under a [CC-BY-NC-ND 4.0 International license](https://creativecommons.org/licenses/by-nc-nd/4.0/).







GH region	$MD_{sec} [dB] \equiv \left[ \frac{1}{n} \times \sum_{i=1}^n \frac{TD_i}{s_i^2} \right] \Big/ \left[ \frac{1}{52} \times \sum_{i=1}^{52} \frac{1}{s_i^2} \right]$	$PSD_{sec} [dB] \equiv \left[ \frac{1}{n} \sum_{i=1}^n s_i^2 \right] \left[ \frac{1}{n-1} \sum_{i=1}^n \frac{(TD_i - MD_{sec})^2}{s_i^4} \right]$
Normal standard deviation [dB]		
 <p>inferonasal</p>	$MD_{\text{inferonasal}} = \left[ \frac{TD_9/(4.3)^2 + TD_{17}/(4.7)^2 + TD_3/(4.4)^2 + \dots + TD_9/(3.2)^2 + TD_{10}/(2.9)^2 + TD_{17}/(3.1)^2}{1/(4.3)^2 + 1/(4.7)^2 + 1/(4.4)^2 + \dots + 1/(2.6)^2 + 1/(2.6)^2 + 1/(2.7)^2} \right]$	$1/8 \times [(4.3)^2 + (4.7)^2 + \dots + (2.9)^2 + (3.1)^2] \times \left[ \frac{(TD_9 - MD_{\text{inferonasal}})^2}{(4.3)^2} + \frac{(TD_{17} - MD_{\text{inferonasal}})^2}{(4.7)^2} + \dots + \frac{(TD_{10} - MD_{\text{inferonasal}})^2}{(2.9)^2} + \frac{(TD_{17} - MD_{\text{inferonasal}})^2}{(3.1)^2} \right]$
 <p>inferotemporal</p>	$MD_{\text{inferotemporal}} = \left[ \frac{TD_6/(3.0)^2 + TD_7/(2.8)^2 + TD_8/(3.1)^2 + \dots + TD_{20}/(2.6)^2 + TD_{21}/(2.1)^2 + TD_{22}/(2.0)^2}{1/(4.3)^2 + 1/(4.7)^2 + 1/(4.4)^2 + \dots + 1/(2.6)^2 + 1/(2.6)^2 + 1/(2.7)^2} \right]$	$1/12 \times [(3.0)^2 + (2.8)^2 + \dots + (2.1)^2 + (2.0)^2] \times \left[ \frac{(TD_6 - MD_{\text{inferotemporal}})^2}{(3.0)^2} + \frac{(TD_7 - MD_{\text{inferotemporal}})^2}{(2.8)^2} + \dots + \frac{(TD_{21} - MD_{\text{inferotemporal}})^2}{(2.1)^2} + \frac{(TD_{22} - MD_{\text{inferotemporal}})^2}{(2.0)^2} \right]$
 <p>temporal</p>	$MD_{\text{temporal}} = \left[ \frac{TD_{23}/(1.9)^2 + TD_{24}/(1.9)^2 + TD_{25}/(2.3)^2 + TD_{32}/(1.7)^2 + TD_{33}/(1.8)^2 + TD_{34}/(2.0)^2}{1/(4.3)^2 + 1/(4.7)^2 + 1/(4.4)^2 + \dots + 1/(2.6)^2 + 1/(2.6)^2 + 1/(2.7)^2} \right]$	$1/6 \times [(1.9)^2 + (1.9)^2 + \dots + (1.8)^2 + (2.0)^2] \times \left[ \frac{(TD_{23} - MD_{\text{temporal}})^2}{(1.9)^2} + \frac{(TD_{24} - MD_{\text{temporal}})^2}{(1.9)^2} + \dots + \frac{(TD_{33} - MD_{\text{temporal}})^2}{(1.8)^2} + \frac{(TD_{34} - MD_{\text{temporal}})^2}{(2.0)^2} \right]$
 <p>nasal</p>	$MD_{\text{nasal}} = \left[ \frac{TD_{18}/(3.5)^2 + TD_{27}/(3.4)^2 + TD_{36}/(2.9)^2 + TD_{44}/(3.3)^2}{1/(4.3)^2 + 1/(4.7)^2 + 1/(4.4)^2 + \dots + 1/(2.6)^2 + 1/(2.6)^2 + 1/(2.7)^2} \right]$	$1/4 \times [(3.5)^2 + (3.4)^2 + (2.9)^2 + (3.3)^2] \times \left[ \frac{(TD_{18} - MD_{\text{nasal}})^2}{(3.5)^2} + \frac{(TD_{27} - MD_{\text{nasal}})^2}{(3.4)^2} + \frac{(TD_{36} - MD_{\text{nasal}})^2}{(2.9)^2} + \frac{(TD_{44} - MD_{\text{nasal}})^2}{(3.3)^2} \right]$
 <p>superotemporal</p>	$MD_{\text{superotemporal}} = \left[ \frac{TD_{29}/(2.3)^2 + TD_{30}/(2.2)^2 + TD_{31}/(1.7)^2 + \dots + TD_{42}/(2.3)^2 + TD_{47}/(2.1)^2 + TD_{48}/(2.1)^2}{1/(4.3)^2 + 1/(4.7)^2 + 1/(4.4)^2 + \dots + 1/(2.6)^2 + 1/(2.6)^2 + 1/(2.7)^2} \right]$	$1/10 \times [(2.3)^2 + (2.2)^2 + \dots + (2.1)^2 + (2.1)^2] \times \left[ \frac{(TD_{29} - MD_{\text{superotemporal}})^2}{(2.3)^2} + \frac{(TD_{30} - MD_{\text{superotemporal}})^2}{(2.2)^2} + \dots + \frac{(TD_{47} - MD_{\text{superotemporal}})^2}{(2.1)^2} + \frac{(TD_{48} - MD_{\text{superotemporal}})^2}{(2.1)^2} \right]$
 <p>superonasal</p>	$MD_{\text{superonasal}} = \left[ \frac{TD_{28}/(1.8)^2 + TD_{27}/(2.6)^2 + TD_{46}/(3.0)^2 + \dots + TD_{32}/(2.6)^2 + TD_{33}/(3.6)^2 + TD_{34}/(2.7)^2}{1/(4.3)^2 + 1/(4.7)^2 + 1/(4.4)^2 + \dots + 1/(2.6)^2 + 1/(2.6)^2 + 1/(2.7)^2} \right]$	$1/11 \times [(1.8)^2 + (2.6)^2 + \dots + (2.6)^2 + (2.7)^2] \times \left[ \frac{(TD_{28} - MD_{\text{superonasal}})^2}{(1.8)^2} + \frac{(TD_{32} - MD_{\text{superonasal}})^2}{(2.6)^2} + \dots + \frac{(TD_{33} - MD_{\text{superonasal}})^2}{(3.6)^2} + \frac{(TD_{34} - MD_{\text{superonasal}})^2}{(2.7)^2} \right]$

Table 1. The sectors (Garway-Heath) with the standard deviation for normal variability each VF location (24-2) (left) with the corresponding calculations for the  $MD_{sec}$  and  $PSD_{sec}$  (middle, right), resp.(17)

As seen in Figure 2, it appears the  $PSD_{loc}$  retains the progression sensitivity throughout the entire perimetric range (18). This is most apparent comparing the two plots at the early ( $0 > MD > -6[dB]$ ) and advanced ( $MD < -25[dB]$ ) range. The information gained from remapping the  $MD_{loc}$  with the sum of the local pattern standard deviations  $PSD_{loc}$  from sectors ( $PSD_{sec}$ ) needs further investigation as now the criteria for staging disease subgroups from the  $PSD_{loc}$  has changed. Finally though visual inspection suggests these regional derived summary indices may offer additional information for the structure function of the progression for glaucoma (12), the traditional global summary statistics still maintain their importance for the overall baseline functional assessment (19, 20).

1. J. Caprioli, L. Mohamed, E. Morales, A. Rabiolo, N. Sears, H. Pradtana, R. Alizadeh, F. Yu, A. A. Afifi, A. L. Coleman, and K. Nouri-Mahdavi. A Method to Measure the Rate of Glaucomatous Visual Field Change. *Transl Vis Sci Technol*, 7(6):14, Nov 2018.

2. D. C. Hood, A. A. Thenappan, E. Tsamis, J. M. Liebmann, and C. G. De Moraes. An Evaluation of a New 24-2 Metric for Detecting Early Central Glaucomatous Damage. *Am J Ophthalmol*, 223:119–128, Mar 2021.

3. S. K. Gardiner and S. Demirel. Detecting Change Using Standard Global Perimetric Indices in Glaucoma. *Am J Ophthalmol*, 176:148–156, Apr 2017.

4. A. Heijl, M. Patella, and B. Bengtsson. *The Field Analyzer Primer: Excellent Perimetry, 5th Edition*. Carl Zeiss Meditec, Inc, Mar 2021.

5. J. Caprioli, D. Mock, E. Bitrian, A. A. Afifi, F. Yu, K. Nouri-Mahdavi, and A. L. Coleman. A method to measure and predict rates of regional visual field decay in glaucoma. *Invest Ophthalmol Vis Sci*, 52(7):4765–4773, Jul 2011.

6. E. Hodapp, I.I.R.K. Parrish, and Douglas Anderson. Clinical decisions in glaucoma. st. louis: Cv mosby comp. *Clinical Decisions in Glaucoma, the CVMosby Co*, pages 52–61, 01 1993.

7. G. Montesano, A. Chen, R. Lu, C. S. Lee, and A. Y. Lee. UWHVF: A Real-World, Open Source Dataset of Perimetry Tests From the Humphrey Field Analyzer at the University of Washington. *Transl Vis Sci Technol*, 11(1):2, Jan 2022.

8. GitHub repository:UWHVF. <https://github.com/uw-biomedical-ml/uwhvf>, 2022.

9. D. C. Hood and C. G. De Moraes. Challenges to the Common Clinical Paradigm for Diagnosis of Glaucomatous Damage With OCT and Visual Fields. *Invest. Ophthalmol. Vis. Sci.*, 59(2):788–791, 02 2018.

10. D. C. Hood and R. H. Kardon. A framework for comparing structural and functional measures of glaucomatous damage. *Prog Retin Eye Res*, 26(6):688–710, Nov 2007.

11. D. F. Garway-Heath, D. Poinoosawmy, F. W. Fitzke, and R. A. Hitchings. Mapping the visual field to the optic disc in normal tension glaucoma eyes. *Ophthalmology*, 107

- 155 (10):1809–1815, Oct 2000.
- 156 12. O. Tan, D. S. Greenfield, B. A. Francis, R. Varma, J. S. Schuman, and D. Huang.
- 157 Estimating Visual Field Mean Deviation using Optical Coherence Tomographic Nerve
- 158 Fiber Layer Measurements in Glaucoma Patients. *Sci Rep*, 9(1):18528, 12 2019.
- 159 13. University of iowa: Collection of perimetric formulas. [http://webeye.ophth.uiowa.edu/](http://webeye.ophth.uiowa.edu/ips/GEN-INFO/standards/standards2010/CollectionOfPerimetricFormulas.pdf)
- 160 [ips/GEN-INFO/standards/standards2010/CollectionOfPerimetricFormulas.pdf](http://webeye.ophth.uiowa.edu/ips/GEN-INFO/standards/standards2010/CollectionOfPerimetricFormulas.pdf), 2010.
- 161 14. O. M. Crook, C. M. Mulvey, P. D. W. Kirk, K. S. Lilley, and L. Gatto. A Bayesian mixture
- 162 modelling approach for spatial proteomics. *PLoS Comput Biol*, 14(11):e1006516, Nov
- 163 2018.
- 164 15. S. K. Gardiner and S. L. Mansberger. Detection of functional deterioration in glaucoma
- 165 by trend analysis using comprehensive overlapping clusters of locations. *Sci Rep*, 10
- 166 (1):18470, 10 2020.
- 167 16. G. Montesano, D. F. Garway-Heath, G. Ometto, and D. P. Crabb. Hierarchical Cen-
- 168 sored Bayesian Analysis of Visual Field Progression. *Transl Vis Sci Technol*, 10(12):4,
- 169 Oct 2021.
- 170 17. A. Heijl, G. Lindgren, and J. Olsson. Normal variability of static perimetric thresh-
- 171 old values across the central visual field. *Arch Ophthalmol*, 105(11):1544–1549, Nov
- 172 1987.
- 173 18. F. Otarola, A. Chen, E. Morales, F. Yu, A. Afifi, and J. Caprioli. Course of Glaucoma-
- 174 tous Visual Field Loss Across the Entire Perimetric Range. *JAMA Ophthalmol*, 134(5):
- 175 496–502, May 2016.
- 176 19. R. P. Mills, D. L. Budenz, P. P. Lee, R. J. Noecker, J. G. Walt, L. R. Siegartel, S. J.
- 177 Evans, and J. J. Doyle. Categorizing the stage of glaucoma from pre-diagnosis to
- 178 end-stage disease. *Am J Ophthalmol*, 141(1):24–30, Jan 2006.
- 179 20. P. Brusini. Staging systems for visual field damage classification in glaucoma. *Eye*
- 180 (*Lond*), 35(8):2324, Aug 2021.

DRAFT